Air-plasma spraying colloidal solutions of nanosized ceramic powders

ZUN CHEN, RODNEY W. TRICE
School of Materials Engineering, Purdue University
E-mail: rtrice@ecn.purdue.edu

M. BESSER, XIAOYUN YANG, D. SORDELET
Metal and Ceramic Sciences Program, Ames Laboratory (USDOE), Iowa State University, Ames, Iowa

Coatings prepared from nanosized powders were obtained by spraying ethanol-based colloidal solutions into a plasma plume. The powders investigated included 40 nm γ-Al$_2$O$_3$, 75 nm 8 wt% Y$_2$O$_3$-ZrO$_2$, and 750 nm 25 wt% CeO$_2$-ZrO$_2$. Spray distances from approximately 50 to 63 mm were required to achieve significant coating deposition. As observed in the TEM, the typical lamella morphology of air plasma sprayed oxide coatings was not observed in coatings fabricated from 40 nm γ-Al$_2$O$_3$, which was comprised of spherical powders that had partially sintered. However, lamellae were observed in the coatings prepared with both nanosized zirconia powders. The characteristic size of the lamella and the grains that comprised the zirconia coatings were nominally a few nanometers. © *2004 Kluwer Academic Publishers*

1. Introduction
The state-of-the-art plasma spray process for ceramics employs large ceramic powders (often greater than 50 μm) that are fed into a plasma plume [1, 2]. The powders are fed through a long supply hose via gas flow into an injector that is located very near the plasma plume; for ceramic powders, the injector is most often located within the plasma gun (i.e., internal injection) to allow direct injection into the plasma plume. As the powder particles are directed into the plume, they are melted and propelled at high velocities onto the surface to be coated, spreading out to form thin "splats" or lamellae structures that comprise the coating [3]. Ideally, one powder particle should result in one lamella; however, some powder particles pass through the plume and are not melted. Lamellae are typically 0.2–0.3 μm thick, with each comprised of hundreds of columnar grains which are nominally 200–300 nm in diameter and oriented parallel with respect to the spray direction. Within the coating, which is essentially made up of numerous lamellae stacked on top of one another, there can be 10–20% porosity, as well as numerous microcracks and mesocracks, most of which appear to be due to stresses generated during cooling.

One of the disadvantages of the conventional plasma spray process is that powders greater than about 10 μm are required to flow properly through a typical powder feeder; powders smaller than these tend to agglomerate due to dominant electrostatic forces unless their surfaces are treated to reduce this attraction. Agglomerated powders clog the supply hose or the injector; moreover, small diameter powders do not typically achieve sufficient momentum transfer from the

plasma. It may, however, be desirable to spray powders much smaller than 10 μm, with the expectation that smaller powders will result in a both smaller lamellae, and possibly smaller grains. The motivation for this work is that early results indicate that nanocrystalline microstructures in coatings improve resistance to thermal cycling [4] in thermal barrier applications.

One approach to create coatings with nanocrystalline features being developed [4–6] is to inject liquids containing ceramic precursors (e.g., aqueous salts) into the plasma. While entrained there, the precursor is converted to crystalline particulates that form via pyrolysis. These newly formed particulates sinter, and ultimately form a nanocrystalline coating. Other researchers [7, 8] have started with nanosized powders that were then agglomerated into larger powders via spray drying. These large powder clusters can then be fed into the plasma plume using conventional feeding methods. By careful control of the spray parameters, the nanosized features can be retained.

The current work focuses on another approach to fabricate coatings comprised of nanocrystalline features. The process involves injecting colloidal suspensions of nanocrystalline ceramic powders into the plasma plume. The powders investigated include 40 nm γ-Al$_2$O$_3$, 75 nm 8 wt% Y$_2$O$_3$-ZrO$_2$, and 750 nm 25 wt% CeO$_2$-ZrO$_2$. Note that the preceding particle sizes are approximate. During the particles' short residence time in the plasma, the ethanol used to disperse the ceramic powders is vaporized, the powder is melted, and then propelled against the substrate to form the coating. The microstructure of the coating was dependent on the
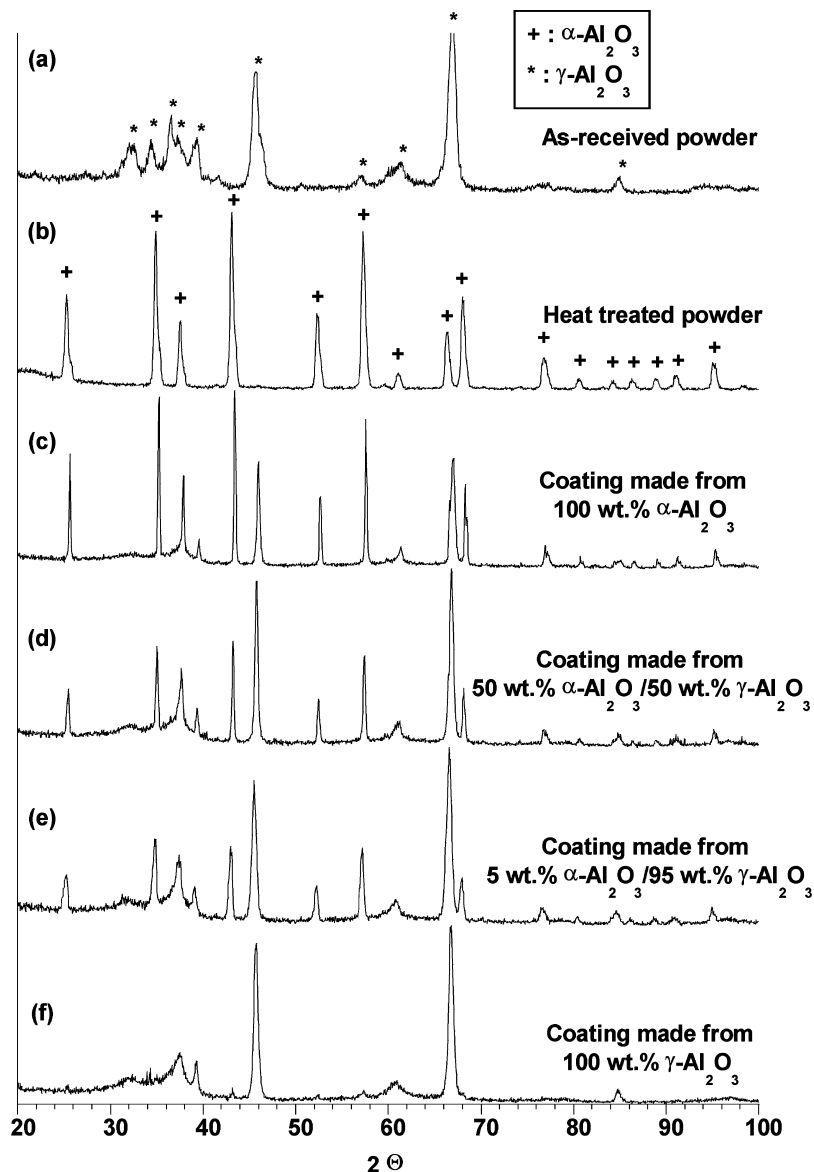
Figure 1 X-ray diffraction results for starting powders and coatings made from alumina slurries. The crystal structure and weight based percentage of α- or γ-alumina starting powder in the slurry is indicated on the plot. The coatings indicated were prepared using a 50 mm spray distance using the NC conditions indicated in Table II.

starting powder composition. Also, the phase assemblage of the Al_2O_3 coatings was strongly influenced by the structure of the starting powders.

2. Experimental procedure
### 2.1. Description of starting powders
The Al_2O_3 powder[1] began with a meta-stable γ-Al_2O_3 crystal structure, a specific surface area of 30–60 m^2/g, and a spherical morphology. Its number-based average diameter was 40 nm as reported by the manufacturer. The crystal structure was verified via X-ray diffraction (XRD) using a Philips PW 1780 laboratory Cu K_α diffractometer. The results are shown in Fig. 1a. To investigate the role of starting powder structure on the phases formed in the coating, a portion of the γ-Al_2O_3 powder was heat treated at 1200°C in air for 0.5 h. XRD indicated that the powder completely converted to the stable α-Al_2O_3 structure (see Fig. 1b). The as-received and heat-treated Al_2O_3 powders were further characterized using a Philips CM30 transmission electron microscope (TEM) operated at 200 kV. Fig. 2a and b are bright field and convergent beam electron diffraction (CBED) micrographs, respectively, taken of the starting γ-Al_2O_3 powder. Note that the powders range in size from 10 to 100 nm. The CBED results presented in Fig. 2b are consistent with the cubic γ-Al_2O_3 phase. As shown in Fig. 2c, the heat-treated particles sintered to an approximate size of 50 to 300 nm. Also, selected area diffraction analysis of the heat treated powder along the [001] zone axis revealed a hexagonal symmetry, consistent with α-Al_2O_3 (see Fig. 2d). During plasma spraying, the flow properties of the heat treated particles were qualitatively the same as the as-received material.
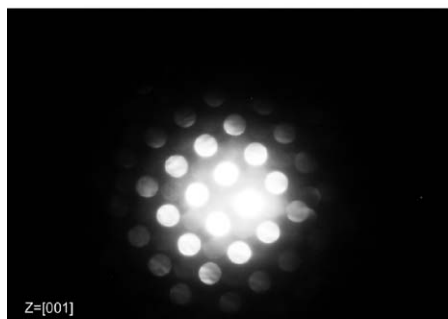
An 8 wt% yttria-stabilized zirconia powder,[2] with an number-based average particle size of 75 nm as determined by a Coulter LS230 particle size analyzer,

---

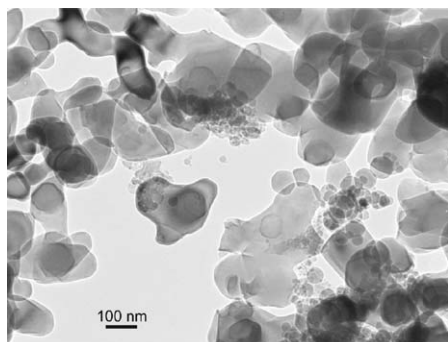[1] Nanophase Technologies Corporation, Product code 100.
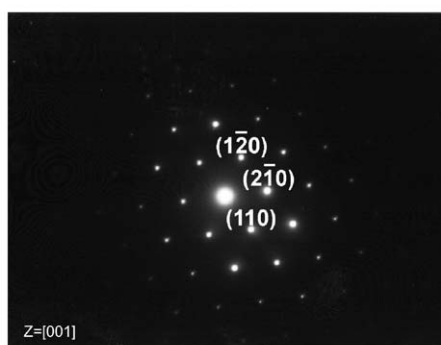
[2] Zirconia Sales, HSY-4.5.
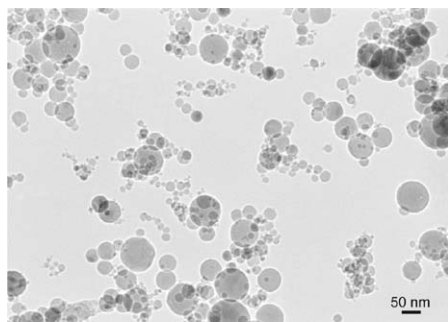
(a)

(b)

(c)

(d)

Figure 2 (a) Bright field TEM image of the as-received γ-Al$_2$O$_3$, (b) CBED pattern for one of the grains indexed along the [001] zone axis consistent with the cubic γ-Al$_2$O$_3$ phase. (c) Bright field TEM image of the heated-treated Al$_2$O$_3$ powder, (d) and a selected area diffraction pattern from one of the grains indexed along [001] zone axes. The observed symmetry is consistent with the hexagonal structure of α-Al$_2$O$_3$.

was also investigated. The initial crystal structure of this commercial powder was tetragonal. The 25 wt% CeO$_2$-ZrO$_2$ powder was fabricated at Purdue University, starting with zirconia[3] and ceria powder.[4] After

[3] Zirconia Sales, DK-2.
[4] Alfa Aesar, REacton stock #11328.

TABLE I Comparison of the amount of heat required to completely vaporize water and ethanol in a 100 gram slurry. Ethanol was used in the current study because less heat was required

Solvent	Moles of solvent[a]	Total heat required to vaporize carrier[b] (kJ/mole)	Total heat required (kJ)
H$_2$O	4.2	43.98	183
C$_2$H$_6$O	1.63	42.32	69

[a]Assuming 75 wt% solvent and 25 wt% yttria-stabilized zirconia.
[b]H$_2$O vaporizes at 100°C; C$_2$H$_6$O vaporizes at 78.3°C.

ball milling these powders for 36 h using zirconia milling media, the dried powder mixture was sintered at 1350°C for 1000 min. X-ray diffraction results revealed that the crystal structure of the ceria-stabilized zirconia powders was predominantly tetragonal, with a small amount (<5 wt%) of cubic phase also observed. Using the Coulter LS 230 particle analyzer, the number-based d_{50} of the sintered powder was measured to be 750 nm.

2.2. Slurry preparation

To prepare a coating with sufficient integrity and thickness, it is important that the solvent be completely vaporized, and that there be sufficient remaining heat in the plasma plume to melt the powder. Two solvents were considered: water and ethanol. Table I shows the amount of heat, beginning at 20°C, required to vaporize either solvent in a 100 gram slurry assuming 75 wt% solvent and 25 wt% yttria-stabilized zirconia. The total heat required to vaporize the water and ethanol was 183 and 69 kJ, respectively [9]. Thus, ethanol was the preferred solvent because less heat was required to vaporize it during its brief time in the plume.

A dispersant[5] was found to be necessary to prepare a stable, deflocculated slurry. Typically, 1 wt% of the dispersant was added to the ethanol solvent, and then the YSZ or alumina powder was added. Slurries were mixed such that the solids loading were 25% by weight. This mixture was ball milled for 10 h to produce the slurry for plasma spraying. All slurries were agitated during plasma spraying using a magnetic stir rod. In this initial study, no attempt was made to measure residual carbon content after spraying; however, as these coatings were prepared in a highly oxidizing environment, the concentration of carbon would be expect to be minimal.

2.3. Apparatus for slurry injection into plasma plume

A 4000 ml stainless steel pressure vessel was used as the holding tank for the slurry. Nitrogen gas at a pressure of 0.3 MPa was used to propel the slurry through the nozzle at a rate of 34 ml/min. Clogging of the nozzle was minimal at this pressure. During injection of the slurry into the plasma plume, the nozzle was tilted back
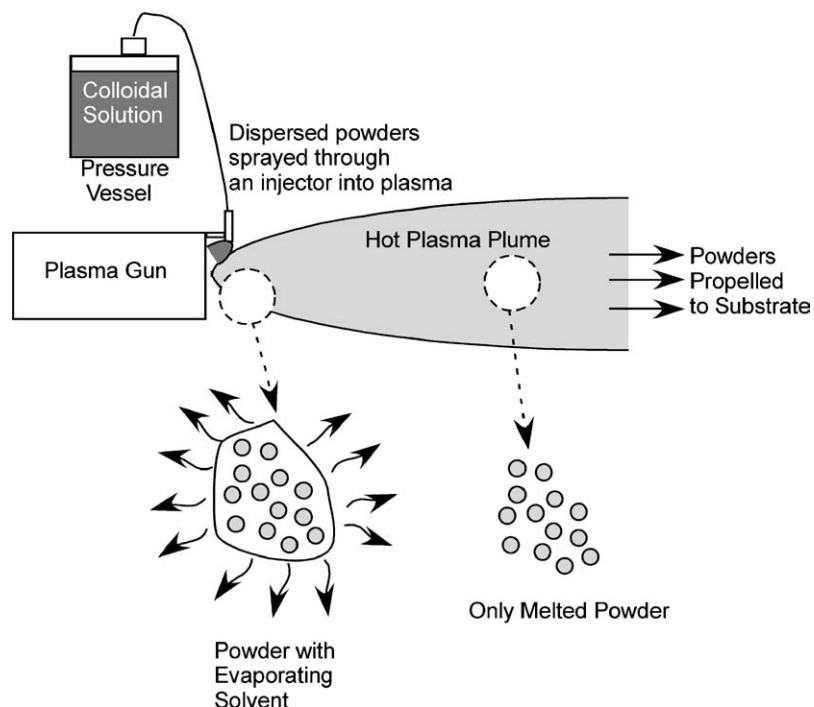
[5] KD-2 from ICI.

Figure 3 Schematic illustration showing injection of colloidally dispersed powder particles into the plasma-plume.

about $10°$ towards the exit of the plasma torch; this arrangement was selected to increase the residence time of the slurry in the plasma plume. The experimental arrangement used in the current study is depicted in Fig. 3.

Air plasma spraying of all slurries was performed at the Ames Laboratory Plasma Spray Facility. For all runs, a Praxair SG-100 gun was assembled with a 145 anode, 129 cathode, and a 113 gas injector, which is commonly used for spraying oxides. Initial coating experiments were performed only using the Al_2O_3 powders. The coating conditions used are described as normal (N), normal with cooling (NC), hot (H), and cold (C); conditions H and C correspond, respectively, to higher and low plasma energies compared to condition N. The plasma spraying conditions are defined in Table II. A wand having two jets attached to the face of the plasma gun that directed air parallel to the plasma axis onto the substrate was used for cooling in the NC and C conditions; moreover, stationary air jets were positioned behind the substrates to increase cooling during deposition. Alumina and zirconia coatings were applied

to stainless steel and copper substrates, respectively, at 50, 63, 75, and 100 mm distances from the plasma gun exit. Sprayed surfaces were grit blasted with 24 grit Al_2O_3 followed by ultrasonic cleaning in ethanol. The x-y manipulator used to control the plasma gun was passed horizontally across the substrate at 100 mm/s, and then moved vertically in 3 mm steps to cover the entire [18 × 30 × 2 mm] substrate. This sequence was repeated 20 times to comprise a complete coating program. However, the program was stopped if the nozzle became clogged or if the slurry was consumed prior to the 20th cycle.

2.4. Specimen preparation and characterization

Coatings were analyzed by XRD similarly to the starting powders. In particular, XRD was used to examine the correlation in phase structure between starting powders and final coatings using powders having various ratios by weight of α-Al_2O_3 and γ-Al_2O_3, and to determine the phase(s) present in the plasma-sprayed zirconia coatings.

TEM specimens of coatings were prepared by first removing the coating from the substrate. Alumina coatings were removed from the steel substrates by deforming the metal substrate; coatings were removed from the copper substrates by etching in hydrochloric acid. Cross-section and plan-view (TEM) specimens were prepared using a tripod polisher.[6] Each specimen was polished progressively using a sequence of 30, 6, and 1 μm diamond coated polishing films for both sides. After transferring the thinned coating to a copper grid, further thinning of the sprayed coatings was performed

TABLE II Overview of the four spray conditions employed in the current work. The plasma was created using a mixture of argon and He

Condition	Normal (N)	Normal with cooling (NC)	Hot (H)	Cold (C)
Current (Amps)	900	900	1200	600
Voltage (Volts)	43.6	43.6	42.2	38
Arc gas, argon (slpm)	70.5	70.5	42.0	150
Auxilliary gas, He (slpm)	42.0	42.0	42.0	0
Slurry pressure (MPa)	0.3	0.3	0.3	0.3
Cooling	None	Wand and jets	None	Wand and jets

---

[6] South Bay Technology, Santa Clara, CA.

4174

using a low-energy ion mill[7] equipped with two hollow anode discharge ion sources that were both set to 4.5 kV and 0.5 mA. The TEM observations on coatings were performed with a Jeol JEM-2000 FX instrument at an accelerating voltage of 200 kV.

Two different coatings prepared with the 8 wt% Y_2O_3-ZrO_2 powder were analyzed using atomic force microscopy (AFM): one coating made from 75 nm powder, the other from 50 μm powder. Specimens oriented to examine their cross section were prepared by polishing both sides of the coating first with 600 grit SiC polishing paper, and then with diamond-coated polishing films down to 1 μm. The samples were subsequently thermally etched at 1200°C for 2 h to reveal boundaries between lamellae and grains. AFM images were obtained using a Digital Instrument Multimode Scanning Probe Microscope[8] in tapping mode.

3. Results and discussion
3.1. Role of spraying distance and spraying conditions

For all powders investigated, deposition was most efficient at a 50 mm spray distance, i.e., at this spray distance the thickest coatings were achieved. With each pass of the plasma gun, approximately 12 μm of coating were applied. Measurable, but lower, deposition rates were obtained at 63 mm. Because of the short spray distances required for significant deposition of the nanosized powders, coatings made at distances of 50 to 63 mm would spall off the substrate unless cooling air was directed to the substrate via the jets described in the experimental procedure (i.e., conditions NC and C). The reason for spallation of the coating was likely poor adhesion of the partially melted powders with the substrate. No measurable coating thickness was obtained in coatings formed using spray distances of 75 and 100 mm.

The NC spray conditions produced the highest quality coatings, as determined by deposition rate and coating integrity (e.g., density as observed by metallography) for all powders investigated. No coatings were successfully formed using the N and H spray conditions (as described in Table II) due to overheating of the substrate and spallation of the coating. The substrate temperature was observed to exceed 400°C at all spray distances for the N and H spray conditions. The C spray condition yielded very low deposition efficiencies, presumably due to decreased solvent vaporization, particle melting or low particle velocity.

3.2. Coatings obtained from alumina slurries

As is well established, γ-Al_2O_3 is one of the intermediate phases formed when alumina is plasma sprayed [10]. Upon cooling from the melting temperature of alumina (2060°C), γ-Al_2O_3 nucleates first over α-Al_2O_3, and thus, plasma-sprayed coatings typically are com-

posed almost entirely of γ-Al_2O_3. Therefore, γ-Al_2O_3 is a marker that can be used to indicate whether the starting α-Al_2O_3 melted in the plume. Fig. 1c–f displays the XRD results of coatings produced from slurries with different amounts of starting α- and γ-Al_2O_3 powders. These coatings were all sprayed at a distance of 50 mm from the substrate using the NC condition. Since the coating fabricated from the slurry composed of 100 wt% α-Al_2O_3 has only a small fraction of γ-Al_2O_3 (see Fig. 1c), the XRD data indicate that only a small amount of powder was melted during spraying.

As shown in Fig. 1d, the coating formed from the 50 wt% α-Al_2O_3/50 wt% γ-Al_2O_3 slurry was comprised of approximately equal amounts of each phase. These estimations were based on comparing integrated X-ray intensities from several powder mixtures having known rations of α-Al_2O_3 and γ-Al_2O_3. Similarly, coatings formed from a slurry composed of 5 wt% α-Al_2O_3/95 wt% γ-Al_2O_3 retained a similar ratio of these two phases (Fig. 1e). The coating made from the slurry with 100% γ-Al_2O_3 was mainly composed of the γ-Al_2O_3 phase (Fig. 1f). Together, the preceding results strongly suggest that the NC plasma spraying
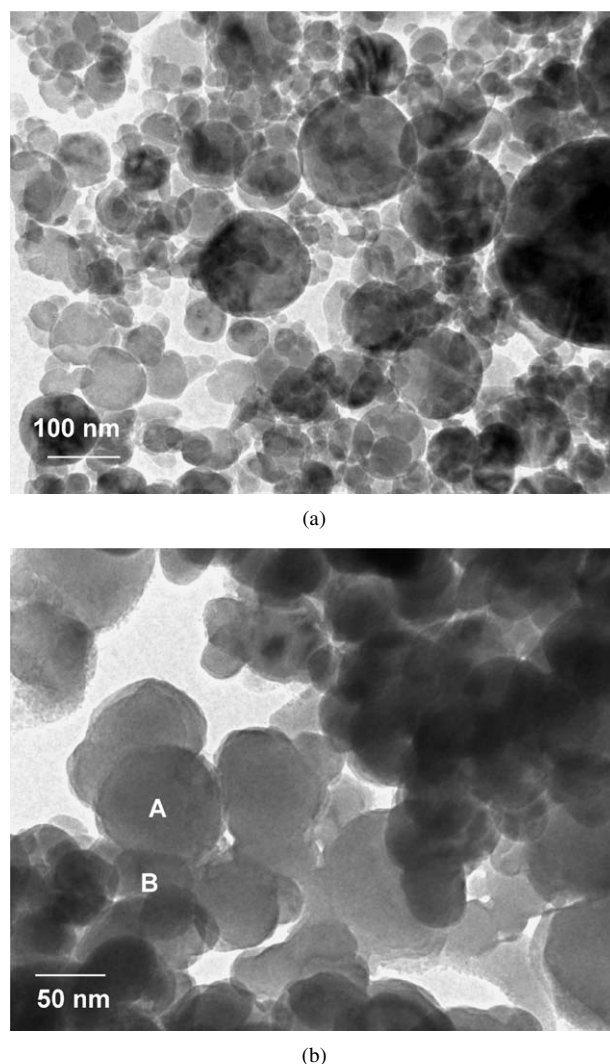

(a)

(b)

Figure 4 Bright field TEM micrograph of a coating prepared by spraying an alumina slurry composed of 50 wt% γ-Al_2O_3/50 wt% α-Al_2O_3 in the plan-view orientation showing: (a) individual powder particles and (b) evidence of sintering between the powder particles labeled A and B.

[7] Gatan®, model DMP 600.
[8] Digital Instruments, Santa Barbara, CA.

conditions, inclusive of the slurry delivery and injection techniques, do not lead to significant melting of the nano-sized alumina powders. As described below, microstructural analysis of the alumina coatings indicates the occurrence of some sintering of powder particles within the plasma plume or after striking the substrate, perhaps in the presence of the plasma as a consequence of the short spraying distance (i.e., 50 mm).

Fig. 4a displays a bright field TEM micrograph of a coating made with a slurry containing 50 wt% α-Al_2O_3/50 wt% γ-Al_2O_3. Individual powder particles having sizes ranging from 20 nm through 200 nm can be clearly distinguished in the micrograph. The spherical morphology of the powders was similar to that observed in the starting γ-Al_2O_3 powder. Thus, it appears that in principle the approach taken to feed the powders into the plume was effective (i.e., the nanosized dimensions are retained). Fig. 4a also reveals that the characteristic lamellar structure normally apparent in plasma-sprayed coatings is not present in the alumina coatings. From the results of the XRD data, it is clear that the reason for this is that most of the powder was not melted, and therefore maintains its spherical shape upon impact with the substrate. Inspection of the coating surface indicated that the coating was fairly abrasion resistant, as determined simply by scratching with a metal file. Thus, the coating demonstrated some strength, implying that the powders were more than loosely agglomerated onto the substrate surface. The coating morphology observed in

Fig. 4b is consistent with this observation, showing two adjacent powder particles that have joined together during the spray process or during subsequent passes of the torch over the coating/substrate.

3.3. Zirconia slurries

Based on the prior results with spraying the alumina slurries, all zirconia powders were sprayed under the NC condition. Fig. 5a and b are the XRD results for the 8 wt% Y_2O_3-ZrO_2 starting zirconia powders and the final coatings produced from the sprayed slurries. The starting 8 wt% Y_2O_3-ZrO_2 powder and the resulting coating have similar tetragonal structures. Analysis of diffraction peaks between 72–76° indicated that an yttrium-rich tetragonal phase was formed [11]. This yttrium-rich tetragonal phase is typically observed when large-diameter yttria-stabilized zirconia powders are plasma sprayed. Similarly, no change between final coating phase composition and the starting powder was observed for the 25 wt% CeO_2-ZrO_2 powder (see Fig. 5c and d). The 25 wt% CeO_2-ZrO_2 powder coating exhibits slightly more peak broadening than the starting powders, which may indicate the these larger particles experienced some degree of melting that led to a reduced grain size during quenching upon impact with the substrate. Further evidence of particle melting during spraying of the zirconia powders was observed during TEM analysis, as discussed below.
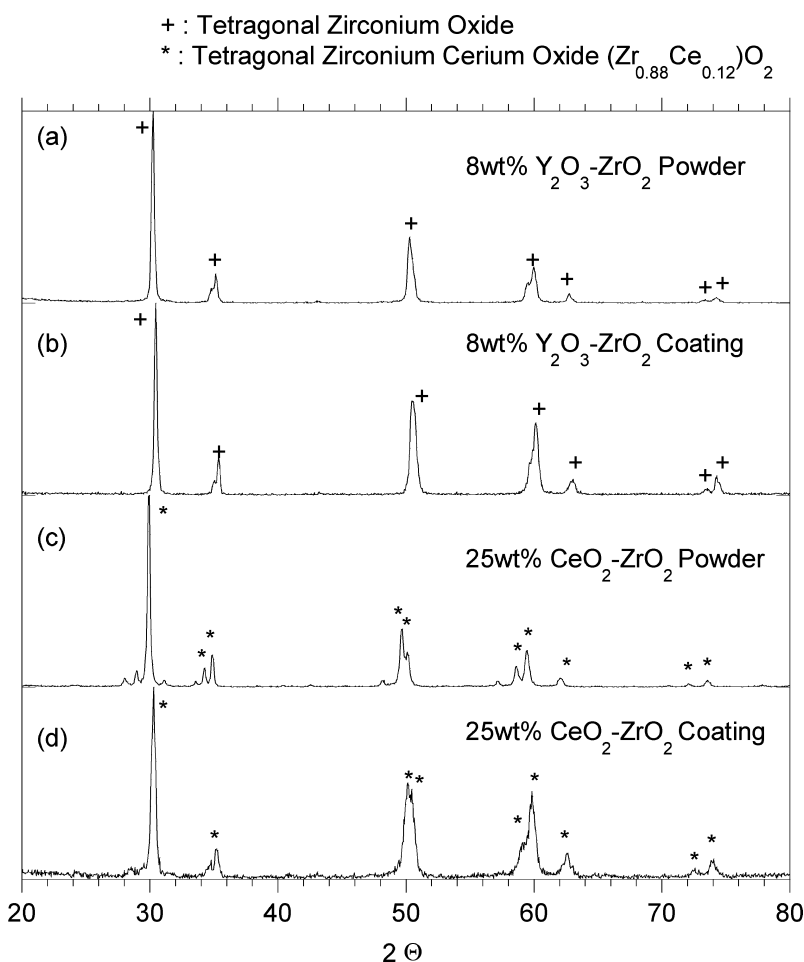

+ : Tetragonal Zirconium Oxide
* : Tetragonal Zirconium Cerium Oxide $(Zr_{0.88}Ce_{0.12})O_2$

Figure 5 X-ray diffraction results for coatings made from the 8 wt% Y_2O_3-ZrO_2 and 25 wt% CeO_2-ZrO_2 slurries. For each composition, the phases observed in the starting powder and coating were the same.
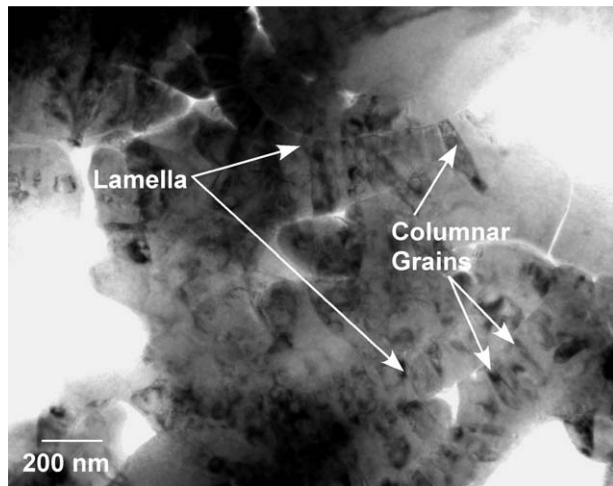
Figure 6 Bright field TEM micrograph of the plasma-sprayed 8 wt% Y$_2$O$_3$-ZrO$_2$ slurry in the plan-view orientation. Note the thin lamella formed during spraying.

Fig. 6 displays a bright field TEM micrograph of a coating made from nano-crystalline 8 wt% Y$_2$O$_3$-ZrO$_2$ powder. This image reveals that the powder particles melted while in the plasma because lamellae or splats are clearly visible; the thin lamellae do not form unless the powders are melted and possess enough kinetic energy to overcome surface tension (and flatten) upon contact with the substrate [12]. In this particular plan-view oriented TEM micrograph, several thin lamellae can be seen. They are typically 100–200 nm thick, and consist of columnar grains with approximate diameters of 20–40 nm. As the starting powder was nominally 75 nm in diameter, it appears that some agglomeration of the powder particles occurred during plasma spraying. However, the features of the coating are still quite small compared to conventional coatings produced with particles generally >20 μm. Although not shown in Fig. 6, unmelted, or perhaps melted and re-solidified particles were observed. Similarly shaped particles are well known to be occasionally present to some degree in conventional zirconia coatings. Fig. 7 is a typical cross-section bright field TEM image from the 25 wt CeO$_2$-ZrO$_2$ coating. Many individual lamellae are present and
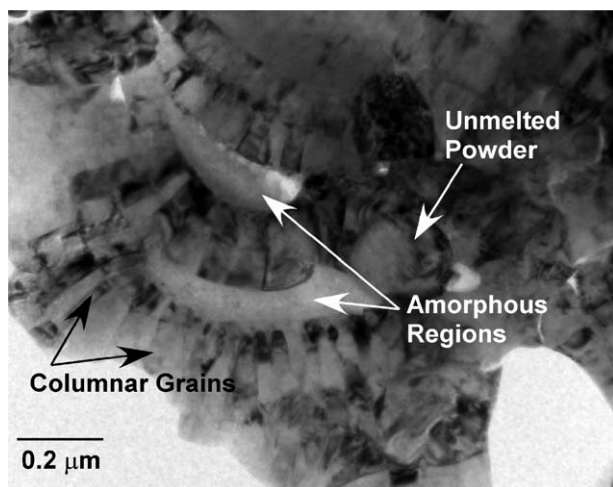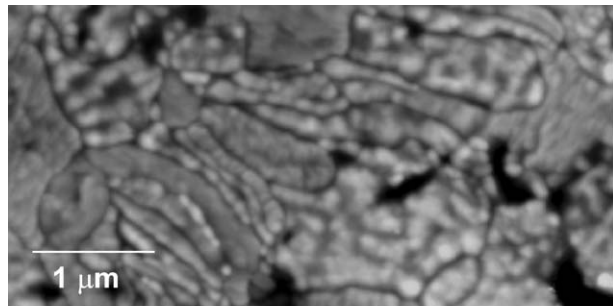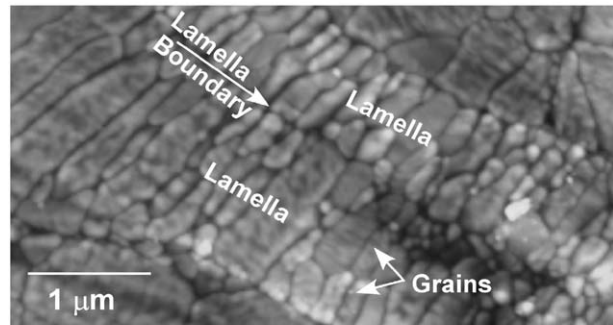

Figure 7 A cross-sectional bright field TEM image of a 25 wt% CeO$_2$-ZrO$_2$ coating with individual lamellae and columnar grains, and an unmelted particle all apparent.

(a)

(b)

Figure 8 Atomic force microscopy results of 8 wt% Y$_2$O$_3$-ZrO$_2$ plasma-sprayed coatings made using (a) colloidal solutions of nanosized 8 wt% Y$_2$O$_3$-ZrO$_2$ and (b) conventionally sprayed (i.e. powder fed) 50 μm diameter 8 wt% Y$_2$O$_3$-ZrO$_2$. Both micrographs are in the cross-sectional orientation.

are built up of grains that are nominally 40–60 nm in diameter. A single large unmelted powder particle was observed, as indicated on the micrograph. Some amorphous regions between the lamella were observed.

3.4. Comparison to conventionally sprayed coatings

Atomic force microscopy was used to compare the cross-sectional microstructure of 8 wt% Y$_2$O$_3$-ZrO$_2$ plasma sprayed coatings prepared in this study to conventionally fed and plasma sprayed 50 μm diameter 8 wt% Y$_2$O$_3$-ZrO$_2$ powders. Prior to testing, each coating was polished to 1 μm and then thermally etched at 1200°C for 0.5 h. The results are shown in Fig. 8. The coating made with the nano-sized zirconia, Fig. 8a, shows multiple lamellae of similar scale to those observed in Fig. 6. In some regions, it is possible to resolve the individual columnar grains. A cross-sectional view of the 50 μm diameter zirconia powders is displayed in Fig. 8b. Only two large lamellae are present, indicating that the lamellae were made from larger powders. Clearly the microstructural features of the coating fabricated from the nanosized powders are finer.

4. Conclusions

Plasma sprayed coatings made from nanosized powders were fabricated and characterized. The powders investigated included 40 nm γ-Al$_2$O$_3$, 75 nm 8 wt%

Y_2O_3-ZrO_2, and 750 nm 25 wt% CeO_2-ZrO_2. Because of the difficulty feeding small powders into a plasma plume, ethanol-based colloidal slurries of each powder were prepared and fed into the plasma using a fine-spray injector under pressurized nitrogen. Coating deposition rates were higher for small spray distances (50 mm) and spray conditions that included cooling for the substrate. Coatings made from the 40 nm γ-Al_2O_3 did not completely melt during spraying, as determined by XRD and TEM investigations. Thus, the microstructure of the coating was comprised of small spherical powders that were partially sintered. TEM observation of coatings made from zirconia powders (both compositions) revealed thin lamellae (100–200 nm thick), evidence that the powders had completely or at least partially melted while in the plasma plume. The grains that made up individual lamellae were much smaller, ranging from 10–40 nm in diameter. Lamellae size seemed to scale with the starting powder size. Some evidence of agglomeration of melted powders in the plume was observed for the zirconia powders.

Acknowledgements

References

1. R. B. HEIMANN, "Plasma-Spray Coating: Principles and Applications" (VCH, 1996).
2. L. PAWLOWSKI, "The Science and Engineering of Thermal Spray Coatings" (Wiley, 1995).
3. R. McPHERSON, *Surf. Coat. Tech.* **39/40** (1989) 173.
4. N. P. PADTURE, K. W. SCHLICHTING,. T. BHATIA, A. OZTURK, B. CETEGEN, E. H. JORDAN, M. GELL, S. JIANG, T D. XIAO, P. R. STRUTT, E. GARCIA, P. MIRANZO and M. I. OSENDI, *Acta Mater.* **49**(12) (2001) 2251.
5. T. BHATIA, A. OZTURK, L. XIE, E. JORDAN, B. CETEGEN, M. GELL, X. MA and N. PADTURE, *J. Mater. Res.* **17**(9) (2002) 2363.
6. G.-M. CHOW, L. K. KURIHARA, T. D. XIAO, P. R. STRUTT, C. W. STROCK and R. A. ZATORSKI, U. S. Patent no. 6,447,848 (2002).
7. L. L. SHAW, D. GOBERMAN, R. REN, M. GELL, S. JIANG, Y. WANG, T. D. XIAO and P. R. STRUTT, *Surf. Coat. Tech.* **130** (2000) 1.
8. H. CHEN and C. X. DING, *ibid.* **150** (2002) 31.
9. "CRC Handbook of Chemistry and Physics", 82nd ed., editor-in-chief, David R. Lide (CRC Press, Boca Raton, FL, 2001–2002) pp. 5–18, 5–31, 6–109, 6–110.
10. R. MCPHERSON, *J. Mater. Sci. Let.* **15** (1980) 3141.
11. K. MURALEEDHARAN, J. SUBRAHMANYAM and S. B. BHADURI, *J. Amer. Ceram. Soc.* **71**(5) (1988) C226.
12. R. McPHERSON, *Thin Solid Films* **83** (1981) 297.